Journal of Materials Chemistry A

ROYAL SOCIETY OF CHEMISTRY

COMMUNICATION

View Article Online
View Journal | View Issue

Cite this: *J. Mater. Chem. A*, 2025, **13**, 9660

Received 16th October 2024
Accepted 16th February 2025

DOI: 10.1039/d4ta07380k

rsc.li/materials-a

A heteroepitaxial interface of Pt//CeO_2 nanoparticles for enhanced catalysis of the oxygen reduction reaction (ORR)†

Nasrat Hannah Shudin,[ab] Ryuto Eguchi,[ac] Shigenori Ueda,[a] Ankit Singh,[a] Ayako Hashimoto *[ac] and Hideki Abe *[ab]

Metal-oxide nanocomposites (MONs) have garnered significant interest in catalysis due to their excellent performance in various chemical reactions. A key focus of research on MONs is the heteroepitaxial metal-oxide interface, which is known to serve as a highly active catalytic center. In this report, we demonstrate that nanometer-sized MONs with heteroepitaxial interfaces can be engineered to exhibit enhanced catalytic performance owing to their strong interfacial effects. Specifically, a MON material composed of platinum (Pt) and cerium dioxide (CeO_2), denoted as Pt//CeO_2, can be obtained by exposing graphene-supported precursor Pt_5Ce alloy nanocrystals (Pt_5Ce/graphene), which are synthesized by the pyrolytic dissociation of chloroplatinic acid (H_2PtCl_6) and cerium trichloride ($CeCl_3$) in a hydrogen-containing atmosphere, to a gas mixture of carbon monoxide (CO) and oxygen (O_2) at elevated temperatures. Transmission electron microscopy (TEM) observations revealed a sharp heteroepitaxial interface between Pt(110) and CeO_2(110) planes within the Pt//CeO_2 material. This nanometer-sized heteroepitaxial interface showed superior catalytic activity of Pt//CeO_2 compared to carbon-supported Pt and large-grained Pt//CeO_2 bulk catalysts for the oxygen reduction reaction (ORR) in basic media.

1 Introduction

Catalysts play a crucial role in the economy, with approximately 90% of chemical manufacturing processes worldwide relying on high-performance catalysts. Among them, heterogeneous nanocatalysts comprising metal-oxide nanocomposites (MONs) are widely used due to their enhanced performance compared to their bulk counterparts.[1–4] The enhanced catalytic performance of MONs is widely attributed to strong interfacial effects that improve electronic transfer and atomic exchanges at the metal-oxide interface.[5–9] The interfacial effects are particularly strengthened at the heteroepitaxial interface, where a pair of the metal-oxide phases is conjugated sharing one or more crystal axes. This heteroepitaxial interface with fewer atomic defects and lattice-mismatch distortions facilitates charge and atomic transfers across the interface, further improving their catalytic performance.[10–12]

Heterogeneous catalysts comprising MONs are typically synthesized as nanoparticles smaller than 100 nanometers to maximize the exposure of active sites for catalysis, using conventional wet chemistry processes involving impregnation methods or co-precipitation methods.[13,14] In both methods, the building blocks for the desired MON nanoparticles, consisting of small molecules and/or nanoparticles, are initially dissolved or highly dispersed in a solvent to form a solution. The solution is then dried, and the resulting solid sediment is typically heated in a controlled atmosphere to produce the desired MON nanoparticles.[15–17] However, a technical challenge arises in synthesizing MON nanoparticles with a catalytically active metal-oxide heteroepitaxial interface *via* wet chemistry approaches where these methods often yield randomly oriented heterointerfaces rather than the desired atomically oriented heteroepitaxial interfaces.

We propose here a hybrid approach for synthesizing MON nanoparticles with metal-oxide heteroepitaxial interfaces. Graphene nanoplatelets are dispersed in an aqueous solution containing chloroplatinic acid (H_2PtCl_6) and cerium trichloride ($CeCl_3$), and subsequently dried to form a solid-state sediment. This sediment is then heated in a stream of hydrogen (H_2) and argon (Ar) gases at 900 °C to precipitate Pt_5Ce alloy nanocrystals on the surface of graphene nanoplatelets, yielding graphene-supported Pt_5Ce nanocrystals. The Pt_5Ce nanocrystals are further treated in a gas mixture of carbon monoxide (CO) and oxygen (O_2) at 600 °C to selectively oxidize Ce atoms, forming the desired Pt–CeO_2 MON nanoparticles with a heteroepitaxial interface (Pt//CeO_2). Transmission electron microscope (TEM) observations reveal that the Pt metal and CeO_2 phases of the Pt//CeO_2 nanoparticles contact at a heteroepitaxial interface.

[a]National Institute for Materials Science, Namiki 1-1, Tsukuba, Ibaraki 305-0044, Japan. E-mail: ABE.Hideki@nims.go.jp; Hashimoto.Ayako@nims.go.jp
[b]Graduate School of Science and Engineering, Saitama University, 255 Shimo-Okubo, Saitama 338-8570, Japan
[c]University of Tsukuba, 1-1-1 Tennodai, Tsukuba, Ibaraki 305-8577, Japan

† Electronic supplementary information (ESI) available. See DOI: https://doi.org/10.1039/d4ta07380k

Catalytic tests for the oxygen reduction reaction (ORR) in aqueous electrolytes have further demonstrated that the Pt//CeO_2 nanomaterial exhibits superior ORR activity compared to the bulk counterpart, Pt//CeO_2 bulk catalyst. This enhancement is attributed to strengthened interfacial effects at the heteroepitaxial interface. The findings of this study highlight the simple approach in obtaining a heteroepitaxial interface in nanomaterials *via* oxidation-triggered nanophase separation.

2 Materials and methods

2.1 Synthesis of Pt_5Ce/graphene nanoplatelets

Pt_5Ce nanocrystals supported on graphene nanoplatelets have been synthesized *via* a two-step approach: impregnation followed by hydrogen reduction. In the first step, chloroplatinic acid hexahydrate ($H_2PtCl_6 \cdot 6H_2O$; Sigma-Aldrich) and cerium(III) chloride heptahydrate ($CeCl_3 \cdot 7H_2O$; Kishida Chemical) were used as precursors. An aliquot of 100 mg graphene nanoplatelets (Sigma-Aldrich) and 50 ml ultrapure water were added as the support material. The mixture was placed in a sealed 100 ml round bottom flask and sonicated with a magnetic stirrer overnight. This was followed by sonication in a bath sonicator for one hour. The mixture was then transferred to a beaker and placed in an oil bath to dry using the double bowl method. In the second step, the dried powder was placed on a graphite boat and transferred into a glass tube for hydrogen reduction. A 5% H_2/Ar gas mixture was supplied, and the reaction was conducted at 900 °C to obtain Pt_5Ce nanocrystals supported on graphene nanoplatelets.

2.2 Synthesis of Pt_5Ce bulk

The Pt_5Ce bulk sample was prepared to explore the effect of dimensionality on catalytic performance. Pt_5Ce alloy was prepared by melting Pt and Ce metals at a mole ratio of 5 : 1 using an arc torch in an argon environment.[5] The obtained ingot was subsequently crushed and sieved to collect particles with an average size of approximately ~50 μm.

2.3 Phase separation in a CO–O_2 gas environment

The graphene-supported Pt_5Ce nanocrystals were placed in a ceramic crucible and heated at 600 °C in a stream of a mixed gas of CO and O_2 (CO : O_2 = 2 : 1 by volume ratio) for 1 minute to induce phase separation of Pt_5Ce, forming the desired Pt//CeO_2 nanoparticles. A similar procedure was applied to the bulk Pt_5Ce alloy but extended to 12 hours, ensuring complete phase separation across its large grain size of 50 μm to produce the Pt//CeO_2 bulk catalyst. Fig. 1 shows the schematic of the synthetic route for Pt//CeO_2 nanoparticles.

2.4 Characterization

The synthesized Pt_5Ce nanocrystals and Pt//CeO_2 nanoparticles supported on graphene nanoplatelets were characterized using powder X-ray diffraction (pXRD; PANalytical X'Pert Pro (Cu Kα, 45 kV, 30 mA)) over a 2θ range of 0° to 90°. The elemental composition and structure were observed using an aberration-corrected TEM (JEM-ARM200F, JEOL Ltd, Japan) with an energy-dispersive X-ray spectrometer (EDS, JED-2300, JEOL Ltd, Japan). Hard X-ray photoemission spectroscopy (HAXPES) with synchrotron radiation X-rays (5.95 keV) was performed at BL09XU of SPring-8 (Super Photon Ring 8, Hyōgo Prefecture, Japan).

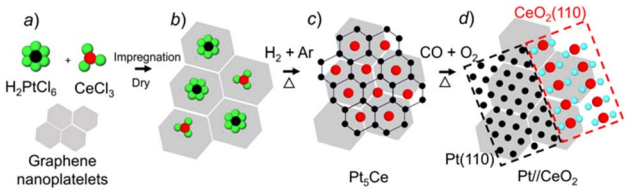

Fig. 1 Schematic of the synthesis route. (a) The materials, (b) impregnation of molecular precursors over graphene nanoplatelets, (c) development of precursor alloy Pt_5Ce nanocrystals, and (d) formation of Pt//CeO_2 nanoparticles through promoted nanophase separation of Pt_5Ce nanoparticles. The (110) planes of Pt and CeO_2 are epitaxially oriented.

2.5 Electrochemical measurements

Electrochemical measurements were conducted using a three-electrode cell connected to a potentiostat (CHI 842B). A 5 mm diameter glassy carbon electrode was used as the working electrode, an Ag/AgCl electrode was used as the reference electrode and a 1 mm diameter Pt electrode was used as the counter electrode. A mixture of ultrapure water (370 μL), isopropanol (100 μL), Nafion solution (5 μL), and the catalyst powder (2.5 mg Pt content) was prepared and sonicated to obtain ink, which was subsequently dropped onto the working electrode. The loading weight of the catalysts was approximately 0.0316 mg mm^{-2} over the glassy carbon electrode. Electrochemical tests were carried out in 0.1 M KOH solution at room temperature. The electrolyte was first purged with Ar gas for 30 minutes, and cyclic voltammetry (CV) was conducted at a scanning rate of 20 mV s^{-1}. The electrolyte was later purged with O_2 gas for 30 minutes, and linear sweep voltammetry (LSV) for the ORR was conducted at a scanning rate of 1 mV s^{-1}.

3 Results and discussion

3.1 Nanoparticles of Pt_5Ce and Pt//CeO_2 supported on graphene nanoplatelets

The pXRD pattern in Fig. 2a(i) represents Pt_5Ce nanocrystals supported on graphene nanoplatelets, which show peaks that match closely with those of the atomically ordered Pt_5Ce phase (ICDD 01-071-7052), indicating a successful synthesis of the desired phase. After the post-treatment in a CO–O_2 atmosphere for 1 minute, all the peaks corresponding to Pt_5Ce diminished (Fig. 2a(ii)). Instead, the peaks for Pt are clearly observed, suggesting a phase transformation from Pt_5Ce to Pt//CeO_2 has completed within the exposure time.

The HAXPES spectrum in the Pt 4f region for the Pt_5Ce nanocrystals is similar to that for Pt_5Ce bulk in peak positions and intensities (Fig. 2b). The Pt 4f emission peaks for the Pt//CeO_2 nanoparticles show shifts towards lower binding energy compared to the nanocrystals and bulk of Pt_5Ce. The Pt 4f

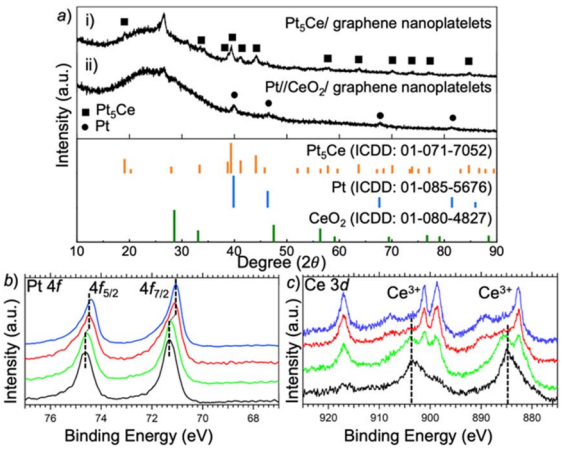

Fig. 2 (a) pXRD of Pt_5Ce nanocrystals and $Pt//CeO_2$ nanoparticles supported on graphene nanoplatelets. (b) HAXPES spectra of the Pt 4f region (blue, red, green, and black curves represent Pt nanoparticles, $Pt//CeO_2$ nanoparticles, Pt_5Ce nanocrystals, and Pt_5Ce bulk, respectively). (c) HAXPES spectra of the Ce 3d region (blue, red, green, and black curves represent CeO_2, $Pt//CeO_2$ nanoparticles, Pt_5Ce nanocrystals, and Pt_5Ce bulk respectively).

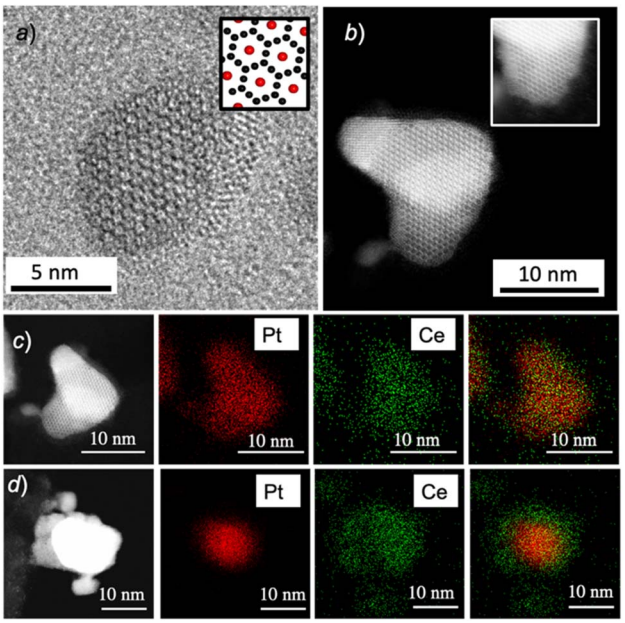

Fig. 3 (a) TEM image of a Pt_5Ce nanocrystal. Inset shows a structural model. The red and black spheres in the inset correspond to the Ce and Pt atoms, respectively. (b) HAADF-STEM image of a Pt_5Ce nanocrystal. Inset shows a filtered STEM image, clearly showing crystal structures. (c) STEM image and EDS mapping of the Pt_5Ce nanocrystal. (d) STEM image and EDS mapping of $Pt//CeO_2$ nanoparticles after phase separation. The red and green regions in the mapping correspond to Pt and Ce, respectively.

spectrum for the $Pt//CeO_2$ nanoparticles is similar to that for pure Pt bulk instead of the Pt_5Ce bulk, indicating the chemical environment for Pt in the $Pt//CeO_2$ nanoparticles is close to that in pure Pt instead of Pt_5Ce. The HAXPES spectrum in the Ce 3d region for the $Pt//CeO_2$ is similar to that for pure CeO_2, unlike any of the spectra for the nanocrystals and bulk Pt_5Ce, indicating that the Ce atoms in $Pt//CeO_2$ are situated in a similar environment in pure CeO_2 instead of Pt_5Ce (Fig. 2c). There are recognized Ce^{3+} 3d emissions from the nanocrystals and bulk Pt_5Ce at 884.5 and 903.8 eV, which are absent in the Ce 3d spectrum for the $Pt//CeO_2$ nanoparticles and pure CeO_2. Ce in Pt_5Ce bulk and nanocrystals primarily exhibits photoelectron peaks at binding energy positions corresponding to Ce^{3+} species, whereas the Ce in $Pt//CeO_2$ and CeO_2 primarily shows peaks at binding energy positions corresponding to Ce^{4+} species. However, in the case of Pt_5Ce nanocrystals, photoelectron peaks corresponding to Ce^{4+} species are also observed. These peaks most likely originated from an impurity containing Ce^{4+} within the Pt_5Ce nanocrystals. (see ESI Table S1†). Summarizing the results of pXRD and HAXPES, we conclude that the Pt_5Ce nanocrystals were fully phase-separated into the $Pt//CeO_2$ nanoparticles by the atmosphere treatment.

Pt_5Ce nanocrystals with a size of approximately 10 nm were observed using a TEM and a high-angle annular dark-field (HAADF) scanning TEM (STEM), as shown in Fig. 3a and b, respectively. Elemental mapping with an EDS in Fig. 3c shows spatially overlapped regions of Pt and Ce, confirming the successful synthesis of the desired Pt_5Ce nanocrystals. ESI Fig. S1† shows the corresponding Fast Fourier Transformation (FFT) patterns and the calculated interplanar distance further confirmed Pt_5Ce nanocrystals. STEM-EDS in Fig. 3d show the full phase separation of Pt_5Ce nanocrystals into $Pt//CeO_2$ nanoparticles, showing a clear contrast between Pt and Ce regions after exposure to an oxidative atmosphere containing O_2. FFT patterns and EDS spectra in ESI Fig. S2† show areas corresponding to Pt and CeO_2 phases further proving that phase separation has completed. Note that a longer duration of 12 hours was required for the bulk Pt_5Ce to achieve complete phase separation (see a cross-sectional STEM image of the fully nanophase-separated $Pt//CeO_2$ bulk material, ESI Fig. S3†). Oxygen species from the atmospheric O_2 likely need more time to diffuse into the inner regions of the Pt_5Ce bulk alloy, which explains the extended exposure time to ensure full phase separation.

3.2 Heteroepitaxial interface of nanosized $Pt//CeO_2$ supported on graphene nanoplatelets

An epitaxial interface was observed in the heterostructure of the $Pt//CeO_2$ nanoparticles, as shown in Fig. 4a. All the $Pt//CeO_2$ nanoparticles exhibited an asymmetrical structure with sharp facets (see ESI Fig. S4†). Phase separation initiated by the spontaneous oxidation of the oxyphilic component, in this case, Ce, resulted in distinct regions of Pt and CeO_2.[18] The white lines in Fig. 4a highlight the crystal facets and lattice planes of the Pt and CeO_2 phases. The configurational relationship between the two phases was verified from the FFT patterns (Fig. 4b–d). The Pt- and CeO_2 phases are both on the $[01\bar{1}]$ zone axis, where the Pt(111) plane is parallel to the $CeO_2(002)$ plane (see Fig. 1d). Fig. 4e depicts a configurational model of the $Pt//CeO_2$ nanoparticle along the $[01\bar{1}]$ direction at the heterointerface. The Pt- and CeO_2 phases are conjugated at their $(01\bar{1})$ planes to form an epitaxial interface, perpendicular to their $[01\bar{1}]$ axes.

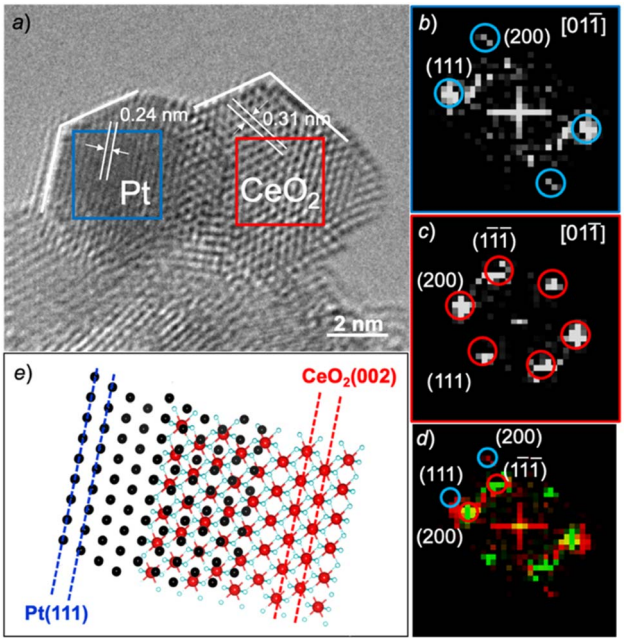

Fig. 4 (a) TEM image of a Pt//CeO_2 particle showing a heteroepitaxial interface. (b–d) FFT patterns from the blue and red squares, and the interface in (a), respectively, demonstrating the configurational relationship between the Pt- and CeO_2 phases. (e) Schematic illustrating the epitaxial (110) interface between the Pt- and CeO_2 phases.

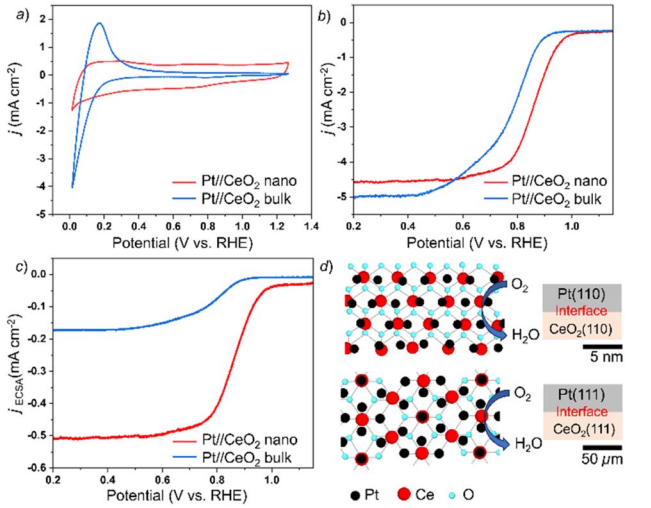

Fig. 5 (a) CV and (b) LSV measurements performed at 1200 rpm in a 0.1 M KOH solution, (c) LSV normalized ECSA and (d) schematic illustrations of the top view and side view of the Pt//CeO_2 interface. The potential was referenced against an Ag/AgCl electrode and then converted to the values for the reversible hydrogen electrode (RHE) for better readability (see the ESI†).

Another configurational relationship, with a parallel relation between the Pt(111) plane and the CeO_2(111) plane as a minor phase, was observed in other nanoparticles having larger grain sizes than 10 nm (ESI Fig. S4†). Note that, in contrast to the nanoparticle system, the epitaxial interface observed in the Pt//CeO_2 bulk system solely showed a Pt(111)//CeO_2(111) relationship.[19] We attribute this difference in configuration to dimension effects, where a larger rotational angle is necessary to accommodate larger particle sizes, resulting in the Pt (111)//CeO_2 (111) relationship.

3.3 ORR catalytic activity

Fig. 5a shows the result of CV in Ar-saturated 0.1 M KOH. The electrochemical surface areas (ECSA) are evaluated as 9.0 m^2 per g Pt for the Pt//CeO_2 nanoparticles and 29.0 m^2 per g Pt for the Pt//CeO_2 bulk catalyst from the area of the hydrogen desorption valley in CV curves (see ESI Fig. S5† for details on the ECSA evaluation). Fig. 5b shows the LSV profiles for the ORR over the different catalysts and Fig. 5c shows the LSV normalized ECSA. CV and LSV for the Pt_5Ce nanocrystals and graphene nanoplatelets are provided in ESI Fig. S6a–c.† The onset potential for the Pt//CeO_2 nanoparticles, +1.01 V *vs.* a reversible hydrogen electrode (RHE), is more positive than those of the Pt//CeO_2 bulk catalyst, +0.91 V *vs.* RHE, and Pt_5Ce nanocrystal, +0.93 V *vs.* RHE (Fig. 5c and S6c ESI†). This positive shift indicates enhanced ORR catalytic activity of the Pt//CeO_2 nanoparticles compared to the bulk Pt//CeO_2 catalyst and Pt_5Ce nanocrystals. The related parameters are compared to electrochemical data of a typically prepared CeO_2-supported Pt catalyst from the literature and provided in ESI Table. S2.† The onset potential was observed to be more positive for Pt(110)//CeO_2(110) nanoparticles compared to other CeO_2-supported Pt catalysts which is likely due to the stronger interfacial effect. We further conducted an electrochemistry test in 1.0 M KOH to evaluate the performance of Pt(110)//CeO_2(110) nanoparticles at different electrolyte concentrations (see ESI Fig. S6d and e†). LSV recorded in 1.0 M KOH in ESI Fig. S6e† shows that the onset potential was observed at +0.88 V *vs.* RHE. There is a shift from +1.01 V *vs.* RHE recorded in 0.1 M KOH. This is expected as by increasing the molar concentration of KOH, the increased OH^- concentration will disrupt oxygen absorption on the active surface. The stability test performed in 0.1 M KOH (ESI Fig. S6f†) shows that the CV curve did not exhibit significant changes after repeated cycles. This suggest that the heterointerface of Pt(110)//CeO_2(110) remains stable throughout the cycle.

Kinetics analysis of the ORR was performed using rotating disk electrode (RDE) voltammetry in O_2 saturated 0.1 M KOH at a different rotating speed with a scanning rate of 1 mV s^{-1}. The current density increases as the rotating speed increases from 100 rpm to 1200 rpm due to the enhanced diffusion of reactants (see ESI Fig. S7a, c and e†). The corresponding K–L plots in Fig. S7b, d and f† indicate the four-electron pathway for all the Pt//CeO_2 nanoparticles, Pt//CeO_2 bulk catalyst and a carbon-supported Pt catalyst (Pt/C, Pt loading: 20 wt%; Fuel Cell Store, Inc).

The HAXPES spectrum in the Pt 4f region for the Pt//CeO_2 nanoparticles exhibits a 74 meV deep-level shift compared to that of pure Pt bulk and the Pt//CeO_2 bulk catalyst (see ESI Fig. S8†). This shift is attributed to a strengthened interfacial effect at the Pt(110)//CeO_2(110) interface in the nanoparticles, as opposed to the Pt(111)//CeO_2(111) interface in the bulk catalyst as shown in the schematic image in Fig. 5d. This enhanced

interfacial effect causes a deep-level shift in the Pt core levels, along with the center of gravity of the Pt d-band in the nanoparticles. Consequently, this deep-level shift in the Pt d-band can weaken the adsorption of intermediate species, such as OH^- anions, near the Pt(110)//CeO_2(110) interface.[20,21] This weakening in the adsorption of reaction intermediates can optimize the balance between mass transfer and electron transfer, leading to the improved ORR activity of the Pt//CeO_2 nanoparticles.[22]

4 Conclusions

A nanometer-sized MON with an epitaxial interface, specifically Pt//CeO_2 nanoparticles, has been successfully synthesized by utilizing the selective oxidation of precursor Pt_5Ce nanocrystals supported on graphene nanoplatelets.[23] The spontaneous nanophase separation of Pt_5Ce nanocrystals results in a (110) epitaxial interface between single-crystalline Pt and CeO_2 phases. The catalytic Pt//CeO_2 nanoparticles exhibit superior ORR activity compared to a carbon-supported Pt catalyst and bulk Pt//CeO_2 catalysts, due to strengthened interfacial effects at the epitaxial Pt(110)//CeO_2(110) interface.

Data availability

Electrochemistry datasets for the catalytic performance test are available at **https://doi.org/10.5281/zenodo.13888952**.

Author contributions

N. H. Shudin synthesized and characterized the nanoparticles. Microscopic observations were conducted by A. Hashimoto, R. Eguchi, and A. Singh. N. H. Shudin, H. Abe, and A. Hashimoto wrote and edited the manuscript. All authors have read and approved the published version of the manuscript.

Conflicts of interest

The authors declare no conflict of interest.

Acknowledgements

The HAXPES experiments were performed at BL09XU of SPring-8 with the approval of the Japan Synchrotron Radiation Research Institute (JASRI) (Proposal No. 2024A1536). AH acknowledges the JST FOREST Program (Grant Number JPMJFR213U) and JST PRESTO (Grant Number JPMJPR17S7) for financial support. HA acknowledges the JSPS Grant-in-Aid for Scientific Research (B) (KAKENHI) (Grant number 22H01799 and 23K23067). This work was supported by "Advanced Research Infrastructure for Materials and Nanotechnology in Japan (ARIM)" of the Ministry of Education, Culture, Sports, Science and Technology (MEXT) (Grant number JPMXP1224NM5122, JPMXP1224NM5255).

References

1 T. W. Van Deelen, C. H. Mejia and K. P. Jong, *Nat. Catal.*, 2019, **2**, 955–970.
2 M. A. Memon, Y. Jang, M. A. Hassan, M. Ajmal, H. Wang and Y. Liu, *Catalysts*, 2023, **13**, 1514.
3 J. Zhang, J. Lian, Q. Jiang and G. Wang, *Chem. Eng. J.*, 2022, **439**, 135634.
4 X. Zhang, Y. Chen, X. Li, Y. Zhang, M. Li, Y. Yang, X. Sun, H. Wang and Y. Xiong, *Catal. Small*, 2021, **17**(42), 2101573.
5 Y. Wen, H. Abe, A. Hirata and A. Hashimoto, *ACS Appl. Nano Mater.*, 2021, **4**, 13602–13611.
6 Q. Fu, H. Saltsburg and M. F. Stephanopoulos, *Science*, 2003, **301**, 935–938.
7 H. Yin, S. Zhao, K. Zhao, A. Muqsit, H. Tang, L. Chang, H. Zhao, Y. Gao and Z. Tang, *Nat. Commun.*, 2015, **6**, 6430.
8 S. Lee, A. Moysiadou, Y. Chu, H. M. Chen and X. Hu, *Energy Environ. Sci.*, 2022, **15**, 206–214.
9 J. Zhang, T. H. M. Pham, Y. Ko, M. Li, S. Yang, C. D. Koolen, L. Zhong, W. Luo and A. Zuttel, *Cell Rep. Phys. Sci.*, 2022, **3**(7), 100949.
10 C. Xu, Y. Wu, S. Li, J. Zhou, J. Chen, M. Jiang, M. Zhao and G. Qin, *J. Mater. Sci. Technol.*, 2020, **40**, 39–46.
11 Y. Luo, Z. Zhang, M. Chhowalla and B. Liu, *Adv. Mater.*, 2021, **34**, 2108133.
12 C. Zhu, A. Wang, W. Xiao, D. Chao, X. Zhang, N. H. Tiep, S. Chen, J. Kang, X. Wang, J. Ding, J. Wang, H. Zhang and H. J. Fan, *Adv. Mater.*, 2018, **30**, 1705516.
13 E. Serena, *Materials*, 2019, **12**(4), 668.
14 J. C. Vedrine, *ChemSusChem*, 2019, **12**, 577–588.
15 J. Song, Y. Yang, S. Liu, L. Li, N. Yu, Y. Fan, Z. Chen, L. Kuai and B. Geng, *Nano Res.*, 2021, **14**(12), 4841–4847.
16 S. B. T. Tran, H. S. Choi, S. Y. Oh, S. Y. Moon and J. Y. Park, *RSC Adv.*, 2018, **8**, 21528–21533.
17 X. Xu, Y. Zhong, M. Wajrak, T. Bhatelia, S. P. Jiang and Z. Shao, *InfoMat*, 2024, **6**, e12608.
18 N. H. Shudin, R. Eguchi, T. Fujita, T. Tokunaga, A. Hashimoto and H. Abe, *Phys. Chem. Chem. Phys.*, 2024, **26**, 14103–14107.
19 Y. Wen, H. Abe, K. Mitsuishi and A. Hashimoto, *Nanoscale*, 2021, **13**, 18987–18995.
20 N. Han, W. Zhang, W. Guo, H. Pan, B. Jiang, L. Xing, H. Tian, G. Wang, X. Zhang and J. Fransaer, *Nano–Micro Lett.*, 2023, **15**, 185.
21 C. Lim, A. R. Fairhurst, B. J. Ransom, D. Haering and V. R. Stamenkovic, *ACS Catal.*, 2023, **13**, 14874–14893.
22 A. Velázquez-Palenzuela, F. Masini, A. Pedersen, M. Escudero-Escribano, D. Deiana, P. Malacrida, T. Hansen, D. Friebel, A. Nilsson, I. Stephens and I. Chorkendorff, *J. Catal.*, 2015, **328**, 297–307.
23 W. Wang, Y. Dong, Y. Yang, D. Chai, Y. Kang and Z. Lei, *J. Hydrogen*, 2018, **43**, 12119–12128.

